43rd AIAA Thermophysics Conference
25 - 28 June 2012, New Orleans, Louisiana

AIAA 2012-2872

# Reconstruction of Mars Pathfinder Aerothermal Heating and Heatshield Material Response Using Inverse Methods

Milad Mahzari[1], Robert D. Braun[2]
*Georgia Institute of Technology, Atlanta, GA, 30332*

Todd R. White[3]
*ERC Inc., Moffett Field, CA 94035*

**The Mars Pathfinder probe entered the Martian atmosphere in 1997 and contained instrumentation that provided measurements of the SLA heatshield subsurface temperature at different locations during the entry sequence. These measurements represented the first Martian aeroheating flight data since the Viking Lander missions. The objective of this paper is to reconstruct the Pathfinder entry vehicle's aerothermal heating and heatshield material response using updated modeling tools and approaches in both direct and inverse manners. The direct approach consists of performing updated Computational Fluid Dynamics (CFD) calculations on a newly reconstructed entry trajectory to characterize the vehicle's heating environment. From the calculated heating boundary conditions, the heatshield in-depth temperature response is computed using an updated thermal response and ablation model for the SLA material. These predictions are compared directly to the flight data. In addition to the direct comparison approach, inverse methods are used to estimate boundary conditions that result in a closer match between the flight data and subsurface temperature predictions. The unblown surface heat transfer coefficient is reconstructed as a function of time using whole-time domain least-squares methods in conjunction with regularization techniques.**

## Nomenclature

| | | |
|---|---|---|
| $B'$ | = | Dimensionless surface blowing rate |
| $C_H$ | = | FIAT heat transfer coefficient = $\rho_e u_e c_h$ |
| $h$ | = | Enthalpy, contact conductance |
| H1 | = | First-order Tikhonov regularization matrix |
| $H_r$ | = | Total recovery enthalpy |
| **J** | = | Sensitivity matrix |
| $\dot{m}$ | = | Surface blowing rate |
| $M$ | = | Number of measurements |
| $N$ | = | Number of discretized $C_H$ points |
| p | = | Pressure |
| **P** | = | Vector of estimation parameters |
| q | = | Heat flux |
| $S$ | = | Sum of square of errors (objective function) |
| t | = | Time |
| T | = | Temperature |
| **T** | = | Vector of direct problem outputs (FIAT predictions) |
| **Y** | = | Vector of measurements |
| $\alpha$ | = | Surface absorptivity |
| $\varepsilon$ | = | Surface Emissivity |

[1] Graduate Research Assistant, Guggenheim School of Aerospace Engineering, AIAA Student Member.
[2] David and Andrew Lewis Professor of Space Technology, Daniel Guggenheim School of Aerospace Engineering, AIAA Fellow.
[3] Research Scientist, Aerothermodynamics Branch, AIAA Member.

$\mu$ = Regularization parameter
$\rho$ = Density
$\sigma$ = Stefan-Boltzmann constant

Subscripts
*c* = Char
*cond* = Conduction
g = Pyrolysis gas
*rad* = Radiative
*w* = Material surface
$\infty$ = Freestream

Superscripts
*k* = Iteration number
*T* = Transpose of a matrix

## I. Introduction

The Thermal Protection System (TPS) is a critical component of most Earth and planetary missions and is responsible for protecting a spacecraft against entry aeroheating. During entry, the interaction between the spacecraft and the planet's atmosphere will generally dissipate more than 90% of the entry system's initial kinetic energy, mostly in the form of heat. Since the TPS is critical to mission success, the aeroheating environment and TPS material response have to be modeled accurately. However, there are substantial uncertainties associated with the analytical models that are currently used for predicting aeroheating and TPS response, such as heating augmentation due to turbulence and catalysis, TPS recession prediction and material properties.[2] These uncertainties have a significant effect on the TPS material selection and total heatshield mass, and therefore limit our ability to design more capable and robust Entry, Descent and Landing (EDL) systems. Flight data can help engineers improve or validate computational tools. During the past few decades, there have been numerous entry missions that were equipped with instruments to collect aeroheating and TPS performance data. A majority of these instrumented missions have occurred in the Earth atmosphere. However, Mars has been and will continue to be a frequent destination in recent space exploration efforts. The MEDLI Integrated Sensor Plug (MISP) instruments on the newly launched Mars Science Laboratory (MSL) mission will provide valuable heatshield subsurface temperature data once it lands in August 2012.[3] To date, Viking and Pathfinder have been the only Mars missions equipped with forebody TPS instruments. The purpose of this paper is to reconstruct the Pathfinder entry vehicle's aerothermal heating environment and heatshield material response using new modeling tools and approaches.

Mars Pathfinder entered the atmosphere of Mars on July 4, 1997. The entry vehicle was a 70 degree spherecone with a 46.6 degree conical backshell. The forebody heatshield material was made of Super-Light Ablator (SLA)-561V, with a nominal thickness of 1.90 cm. The aeroshell was equipped with nine type-K thermocouples and three platinum resistance thermometers at different depths and locations in the heatshield and backshell. In 1999, Milos et al.[1] performed Navier-Stokes heating calculations for the Pathfinder entry vehicle using the Computational Fluid Dynamics (CFD) code GIANTS. They calculated the heatshield material response using three different one-dimensional charring models and directly compared the subsurface temperature flight data and the material response results. The main conclusions of that work was that the stagnation point temperature data were consistent with about 85% of the CFD's fully catalytic laminar heating predictions. Also the shoulder temperature data were consistent with the fully catalytic laminar heating with early onset of turbulence. The bondline temperature data were not of good quality for quantitative analysis and differed greatly from the model predictions.

Building on the work in Reference 1, the objective of this paper is to reconstruct the Pathfinder entry vehicle's aerothermal heating and TPS material response using updated modeling tools and approaches in both direct and inverse manners. The analysis in this paper is only restricted to the forebody instruments, specifically the mid-depth nose and shoulder thermocouples. Section II provides a brief description of the Pathfinder flight experiment and the flight data obtained. In section III, a summary of the previous analysis done by Milos et al. is presented and some of the results relevant to this work are shown. In section IV, a direct analysis is conducted for the Pathfinder vehicle. Based on a newly reconstructed EDL trajectory for the Pathfinder vehicle, updated heating calculations are performed using the NASA CFD code, Data Parallel Line Relaxation (DPLR). [4] From the calculated heating

boundary conditions, the heatshield in-depth temperature response is calculated using an updated thermal response and ablation model for the SLA material and these predictions are compared directly to the flight data. The Fully Implicit Ablation and Thermal Response Program (FIAT)[5] is used in this study to solve the one-dimensional ablation and heat transfer problem. In section V, the analysis is performed in an inverse manner. Inverse methods are used to estimate boundary conditions that result in the closest match between flight data and subsurface temperature predictions. The unblown surface heat transfer coefficient is reconstructed as a function of time using whole time-domain least-squares methods in conjunction with regularization techniques. This paper advances our knowledge of the Mars Pathfinder aerothermodynamic environment and TPS material response by employing: (1) a newly reconstructed trajectory and associated CFD simulations, (2) updated SLA thermal response and ablation model and (3) inverse analysis in addition to direct comparison.

## II. Description of Pathfinder Flight Experiment

The Mars Pathfinder Aeroshell contained nine type-K thermocouples (TC1-TC9) and three platinum resistance thermometers (PRT1-PRT3). Figure 1 from Reference 1 shows a profile view of the aeroshell and the location of the TCs and the PRTs. The PRTs were attached to aluminum blocks and served as isothermal reference junctions for the nine TCs. The TCs were located at different locations and depths in the TPS material (Table 1). Reference 1 provides tables detailing the material stack-up at each TC location.

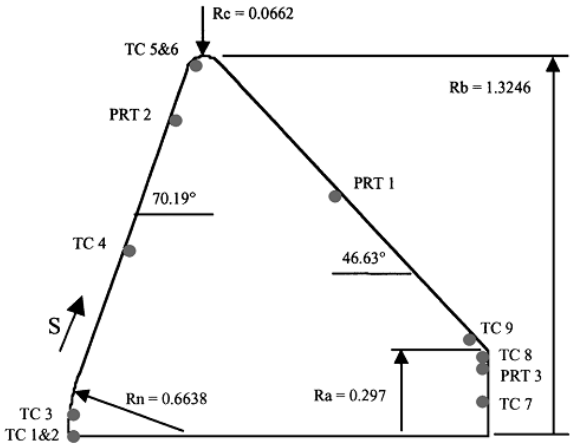


**Figure 1. Pathfinder aeroshell showing the location of the nine thermocouples and three PRTs[1]**

**Table 1. Instrument locations and depths[1]**

| Instrument | *r*, cm | *S*, cm | Depth, cm |
|---|---|---|---|
| T1 | 0.00 | 0.00 | 0.400 |
| T2 | 0.00 | 0.00 | 0.953 |
| T3 | 7.62 | 7.64 | 1.905 |
| T4 | 66.44 | 69.7 | 1.905 |
| T5 | 130.4 | 138.0 | 0.953 |
| T6 | 130.4 | 138.0 | 1.905 |
| T7 | 12.0 | | 0.038 |
| T8 | 27.6 | | 0.038 |
| T9 | 34.0 | | 0.038 |
| PRT1 | 83.9 | 212.5 | 1.340 |
| PRT2 | 110.0 | (inside structure) | |
| PRT3 | 23.5 | (inside structure) | |

There are a number of challenges in the application of this flight data. TC1, TC7 and TC8 did not return any usable data, and possibly failed before or during the launch. The temperature data returned from TC2-6 are known to be incorrect due to the fact that PRT2 measurements were pegged at the low-temperature cutoff of the calibration curve and they were used for the TC data reduction. Reference 1 explains how results from the solar thermal vacuum tests were used to correct the TC data. The conclusion was to subtract 18 ± 2 K from the temperature measurements for TC2-TC6. The analysis done by Milos et al. [1] suggested that the data returned from the bondline thermocouples (TC3, 4 and 6) did not match the temperature profiles predicted by the thermal response models. The measured temperature abruptly rises, then changes slope and shows no resemblance to the predictions. This unusual TC pre-heating behavior has also been seen in arc jet and thermal flash tests and has been attributed to either the evaporation of absorbed moisture[6] or direct transmission of thermal radiation to the bondline.[1] As a result, the focus of this study will be on the mid-TPS thermocouples at nose, TC2, and at the shoulder, TC5.

## III. Summary of the Previous Analysis

Milos et al.[1] calculated CFD heating environments for the entry vehicle using the GIANTS code. The solutions were obtained assuming a radiative equilibrium surface temperature for an unblown fully catalytic wall. Laminar flow was assumed for the nose location, while both laminar and turbulent solutions using an algebraic turbulence model were obtained for the shoulder location. Figure 2 shows the calculated heat flux and the derived convective boundary conditions, $C_H$ and $H_r$, for the nose and shoulder locations.

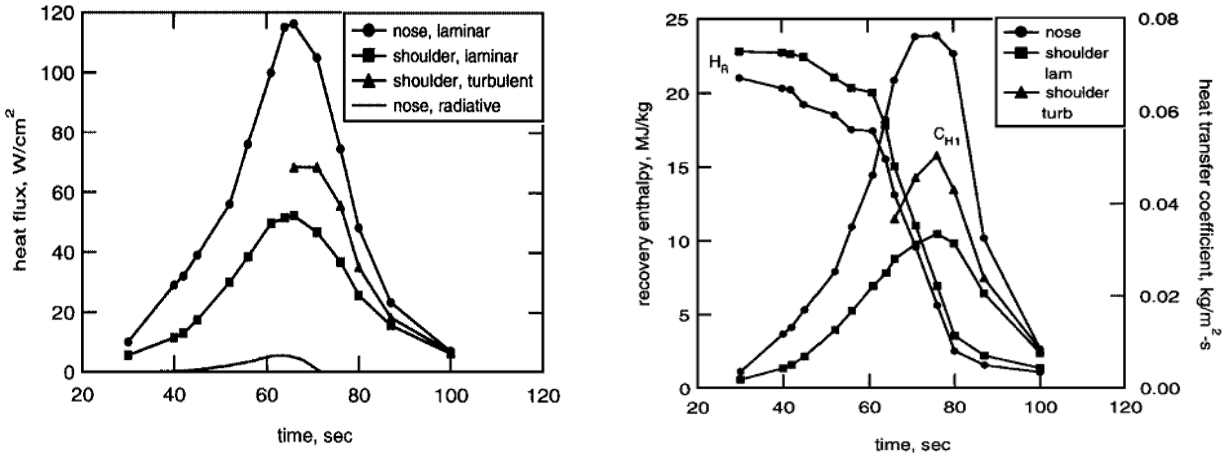


**Figure 2. Pathfinder heating environment calculated by Milos et al.** [1]

Based on these boundary conditions, Reference 1 conducted a one-dimensional material response analysis using three different ablation models. The heat transfer coefficient was extrapolated to zero at 20 and at 101 s. After 101 s the surface was allowed to cool only by reradiation and convective cooling was turned off. A blowing correction approach was used to couple the flow solver solutions to the material response calculations. A laminar boundary condition was used for the nose; the shoulder location was assumed to be laminar with a turbulence onset at 66 s. Figure 3 shows the comparison between flight data at the nose location and the material response calculated using three different models. The results labeled as ARC refer to FIAT calculations done at Ames Research Center. As seen in Figure 3b, the surface heat transfer coefficient was scaled to 85% and it proved to result in a better match with the flight data.

**(a) 100% laminar** **(b) 85% laminar**

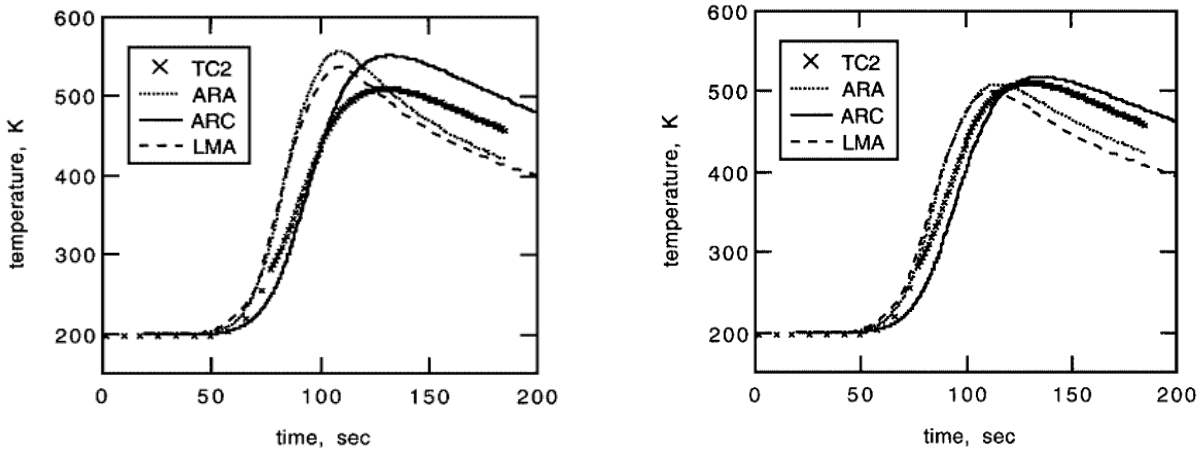


**Figure 3. Pathfinder heatshield material response calculated by Milos et al. for the nose location**[1]

A similar analysis was done for the shoulder location. The material response for laminar heating, turbulent heating after 66s, and 85% turbulent heating environments were computed and were compared to the flight data. Figure 4 shows the results for laminar and 85% turbulent heating cases. It was concluded that both heating cases provided a reasonably good match with the data. We can observe that a rough qualitative match with the data is achieved through the simple scaling approach; however, there is still noticeable difference between the data and thermal response model predictions.

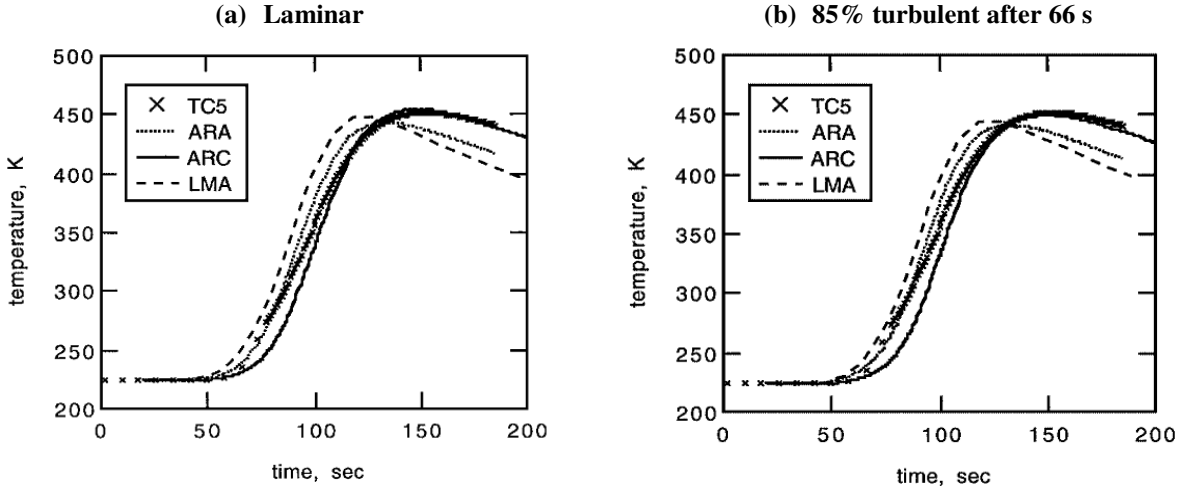


**Figure 4. Pathfinder heatshield material response calculated by Milos et al. for the shoulder location[1]**

## IV. Direct Analysis

In this section, the reconstructed trajectory used in this analysis is first described followed by an explanation of the CFD modeling performed to characterize the vehicle's heating environment. Once the heating boundary conditions are known an in-depth thermal analysis is conducted for the heatshield using FIAT and updated SLA thermal response and ablation model. The predicted TPS temperatures are then compared to the flight thermocouple data.

### A. Trajectory Reconstruction

The previous Mars Pathfinder analysis performed in Reference 1 employed a trajectory reconstructed by Spencer et al.[7] In this paper, a new three degree-of-freedom reconstructed trajectory by Dutta et al.[8] is used. Both trajectories were reconstructed using accelerometer and altimeter data; however the data are processed in different fashions. The trajectory by Spencer et al. is obtained by starting from atmospheric interface conditions from navigational estimations and directly integrating the acceleration measurements in the forward direction using equations of motion; thus, the estimate of measurement uncertainties plays a very small role in the estimation of trajectory states. This process is continued until the altimeter data becomes available. However, there is a discrepancy between the reconstructed trajectory and the altimeter data at the point where this data becomes available. This results in a jump discontinuity in the final reconstructed trajectory as can be seen in the altitude vs. time plot in Figure 5.

In contrast, the trajectory estimation by Dutta et al.[8] is performed by starting with the altimeter data and integrating the equations of motion backward. Note that the reconstruction of the Pathfidner trajectory was first done in this manner by Christian et al.[9] and was subsequently augmented by Dutta et al.'s work. The trajectory is reconstructed using an Extended Kalman Filtering (EKF). The advantage of the backward reconstruction is that the sensor measurements with lower uncertainty such as the altimeter are processed earlier in the estimation and the covariance of the initial state is smaller. The jump discontinuity observed in the case of forward reconstruction is removed as the filter is able to estimate the state first using measurements from the less uncertain altimeter data and then the more uncertain accelerometer data. The altimeter data has an uncertainty of 0.3 m while the atmospheric interface navigational estimate has an uncertainty of few kilometers. Therefore, the backward reconstruction is expected to be closer to the truth trajectory because it weighted towards use of the data of higher confidence. Figure 5 compares the reconstructed trajectory used in Reference 1 and the reconstructed trajectory used in his paper. The reconstruction used in this paper provides the position and velocity of the spacecraft in addition to the atmospheric density and pressure.

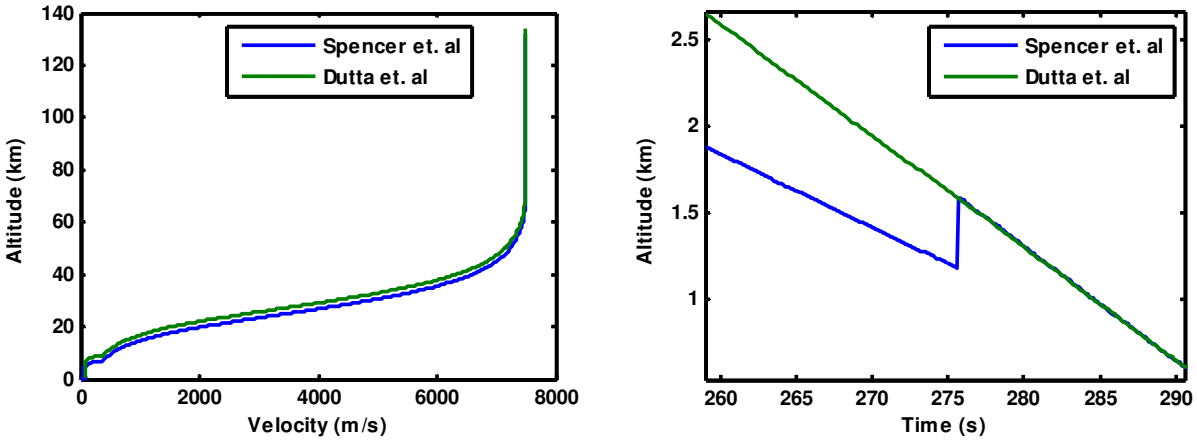


**Figure 5. The reconstructed trajectory used in this paper compared to the one used in Reference 1**

## B. Aerothermal Environment Prediction

This section will describe the methodology used for the calculation of Pathfinder's aerothermal environment based on the newly reconstructed trajectory. The CFD calculations are performed using the DPLR code and current models for the Martian entry. The same methodology described in References 10 and 11 will be used in this study. A series of trajectory points are selected on which DPLR analysis is performed. A total of 21 points along the trajectory are used for CFD analysis covering the range from 25 s to 150 s. Early in the trajectory the flow is expected to be non-continuum therefore Navier-Stokes solutions are not obtained earlier than 25 seconds. Table 2 shows the spacecraft and atmospheric conditions for the selected trajectory points. Figure 6 shows a plot of freestream density and temperature for a subset of these points. The freestream temperature is taken from a separate atmospheric reconstruction done by the Atmospheric Structure Investigation/Meteorology (ASI/MET) experiment science team.[12]

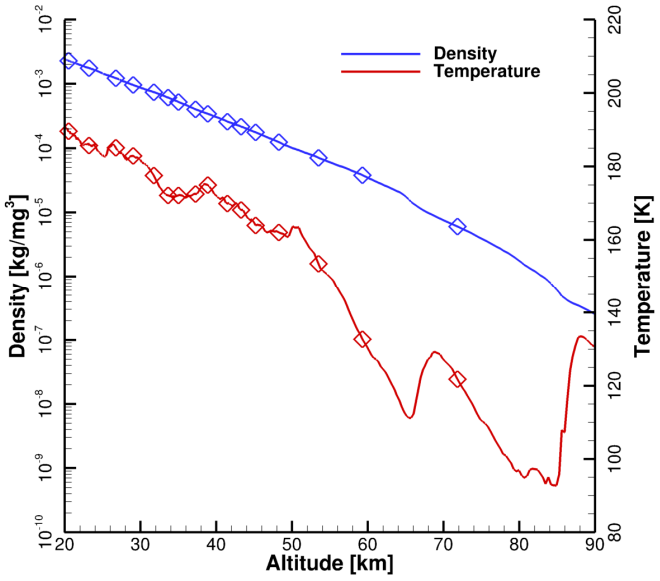


**Figure 6. Mars reconstructed atmospheric properties.[8, 12] Symbols show the subset of trajectory points used for CFD analysis.**

**Table 2. Trajectory points for direct analysis with DPLR**

| Time | Velocity | Altitude | Temperature | Density | Time | Velocity | Altitude | Temperature | Density |
|---|---|---|---|---|---|---|---|---|---|
| *sec* | *m/s* | *km* | *K* | *kg/m3* | *sec* | *m/s* | *km* | *K* | *kg/m3* |
| 25 | 7498 | 93.200 | 127 | 1.70E-07 | 77 | 5171 | 33.632 | 172 | 6.11E-04 |
| 40 | 7492 | 71.819 | 122 | 6.04E-06 | 80 | 4709 | 31.742 | 178 | 7.43E-04 |
| 50 | 7400 | 59.265 | 133 | 3.81E-05 | 85 | 3974 | 29.012 | 183 | 9.61E-04 |
| 55 | 7269 | 53.480 | 154 | 7.11E-05 | 90 | 3312 | 26.736 | 185 | 1.23E-03 |
| 60 | 7051 | 48.255 | 162 | 1.25E-04 | 100 | 2294 | 23.194 | 186 | 1.76E-03 |
| 63 | 6847 | 45.198 | 164 | 1.76E-04 | 110 | 1636 | 20.513 | 190 | 2.28E-03 |
| 65 | 6682 | 43.281 | 168 | 2.16E-04 | 120 | 1211 | 18.308 | 192 | 2.93E-03 |
| 67 | 6491 | 41.447 | 170 | 2.60E-04 | 130 | 925 | 16.363 | 197 | 3.67E-03 |
| 70 | 6157 | 38.860 | 175 | 3.42E-04 | 140 | 725 | 14.560 | 196 | 4.46E-03 |
| 72 | 5903 | 37.249 | 173 | 4.01E-04 | 150 | 577 | 12.830 | 189 | 5.47E-03 |
| 75 | 5476 | 35.008 | 172 | 5.25E-04 | | | | | |

DPLR is a modern, parallel, structured non-equilibrium Navier-Stokes flow solver developed and maintained at NASA Ames Research Center.[4] The code employs a modified Steger-Warming flux-splitting scheme, for higher-order differencing of the inviscid fluxes, and is used here with 2nd order spatial accuracy and to steady-state 1st order in time. DPLR has been validated over a wide spectrum of flight and ground-based experimental simulations. For the following analysis, the flow is solved axisymmetrically which effectively enforces a zero angle of attack and sideslip. The grid employed has 160 cells along the body, and 128 from the surface to the freestream. Each simulation includes several grid alignments to adapt the shock to the strong bow-shock. Figure 7 shows the flowfield temperature distribution at the peak heating point, and laminar and turbulent surface heating predications.

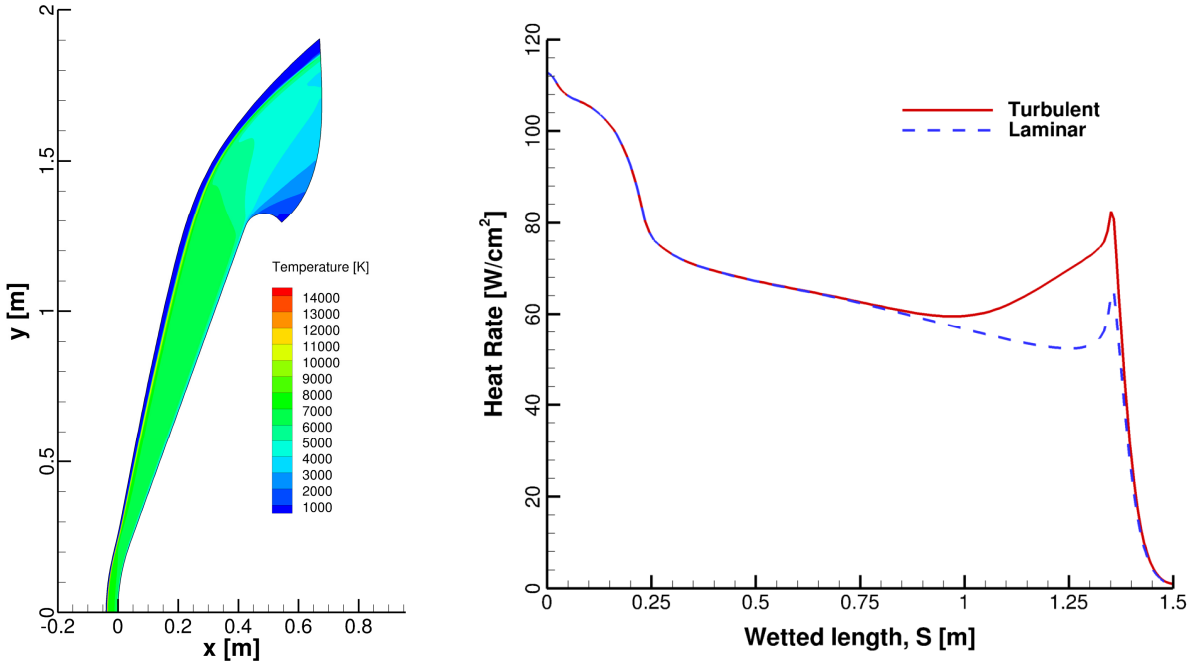


**Figure 7. Flowfield temperatures, and surface heat flux at peak heating (t = 65 sec)**

The flow around the heatshield is modeled as thermochemical non-equilibrium flow, using the Mitcheltree and Gnoffo 8 species 12 reactions Mars model ($CO_2$, CO, $N_2$, $O_2$, NO, C, N, and O).[13] The Mars atmosphere is modeled as 97% $CO_2$ and 3% $N_2$ by mass. The TPS surface is modeled as an unblown non-slip radiative equilibrium wall

with constant emissivity (ε = 0.85) and Mitcheltree and Gnoffo surface catalycity model. This catalycity model assumes maximum recombination of $CO_2$ via the Eley-Rideal mechanism, and is consistent with the "fully catalytic" models used in References 1 and 14. Species diffusion is modeled using self-consistent effective binary diffusion (SCEBD). Turbulent flow is simulated via Menter's shear stress transport (SST) vorticity-based turbulence model with Wilcox blended compressibility correction[15] is used, with a turbulent Schmidt number of 0.7. Previous analysis[1] employed the algebraic Baldwin-Lomax turbulence model. The Baldwin-Lomax model enforces fully turbulent flow over entire heatshield (a conservative design assumption), whereas the SST model includes a turbulent transition model. Radiative heating at the stagnation point is calculated using the same technique as References 1 and 14, and is neglected at the shoulder.

Surface conditions for material response simulations are extracted from the CFD solutions at the stagnation point and shoulder locations (wetted lengths of 0.00 and 138.0 cm, respectively). These quantities are then fitted in time with tight monotonic cubic splines, and provided as inputs to the FIAT material response code at half second intervals. As noted in Reference 1, it is difficult to reliably model convective cooling later in the vehicle's trajectory (t > 100 s). While the overall heating is low, however, CFD simulations were performed after 100 s to provide an initial guess for the inverse analysis presented in Section V. For the current paper, the recovery enthalpy ($H_r$) for FIAT is defined at each CFD point as the free-stream total enthalpy, as shown in Figure 8. Since the formation enthalpy of $CO_2$ at 0 K is negative (-8.93MJ/kg), the freestream total enthalpy becomes negative as the vehicle slows down, and the velocity component of enthalpy decreases.

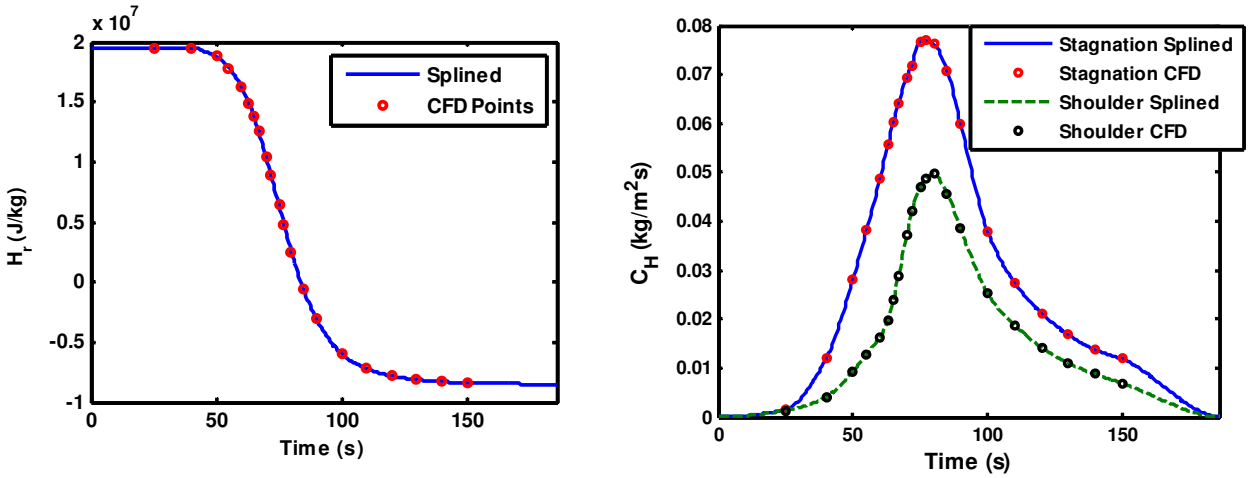


**Figure 8. (a) Recovery enthalpy and (b) Heat-transfer coefficient number from DPLR simulations**

## C. Forebody Heatshield Material Thermal Response

### *1. Thermal Response and Ablation Model*

The current study utilizes the NASA code FIAT[5] with an updated SLA-561V thermal response and ablation model to solve the ablation and heat transfer problem. FIAT is an implicit ablation and thermal response program for simulation of one-dimensional transient thermal energy transport in a multilayer stack of isotropic materials that can ablate from a front surface and decompose in-depth. FIAT has been developed by scientists at the NASA Ames Research Center and is a standard tool in the aerospace industry for the thermal sizing and analysis of spacecraft heatshields. The equations solved in the FIAT code are the internal energy balance, internal decomposition, internal mass balance and surface energy balance equations. The surface energy balance is solved using pre-calculated surface blowing rate, B', tables derived under the assumption of thermochemical equilibrium at the surface.

An important advancement of this work compared to the previous Pathfinder data analysis done by Milos et. al is that an updated thermal response and ablation model is used for SLA-561V. This higher-fidelity model was developed by Laub et. al based on data taken from extensive testing conducted in the NASA Ames IHF and AHF arc jet facilities during 2004-2005.[16] This testing was done in support of the MSL mission and the developed model does not account for potential ablation mechanisms associated with aerodynamic shear, as all the testing were conducted on 4-inch diameter flat-faced cylindrical samples. The updated model consists of two elements: (1) a

thermal response model to predict in-depth temperature response and (2), a surface ablation model to predict surface temperature and surface recession.

SLA-561V is a filled cork silicone in a Flexcore (phenolic fiberglass) honeycomb. It contains an RTV silicone resin, granulated cork, silica and phenolic microballoons, and chopped refrasil fibers. In order to develop an in-depth thermal response model for this material, several thermophysical and thermochemical properties were determined. The density and the decomposition kinetics of the material were developed by Thermo Gravimetric Analysis (TGA). During such testing, the analysis of the material residual mass fraction as a function of temperature allows the identification of separate decomposition reactions. These reactions are described with an Arrhenius relation where the constants are determined from curve fitting the TGA data. The thermophysical properties of the material are determined using mainly lab testing and iterative correlation with a wide range of arc jet test thermocouple data (specifically for char thermal conductivity).

The modeling of TPS ablation is not straight-forward. Empirical correlations based on ground testing cannot be extrapolated to flight conditions with high confidence due to the fact that ground facilities are not capable of simultaneously matching all the flight heating environment parameters (pressure, enthalpy and heat flux). Therefore, Laub et. al[16] focused on the identification of the primary ablation mechanism using thermochemical ablation theory. It was concluded that the surface recession of SLA-561V was mainly due to the vaporization of a molten layer of glass that forms on the surface at the heat fluxes sufficient to melt the glass. Thermochemical equilibrium solutions were generated using the Aerotherm Chemical Equilibrium (ACE) code and were used to iteratively solve the surface energy balance equation to obtain surface temperature and recession. The solutions by this model were checked against arc jet data to demonstrate that this model provides reasonably accurate predictions for a broad range of heating environments. A more detailed discussion of this updated SLA model can be found in Reference 16.

*2. Modeling Assumptions*

The material stack up and thicknesses given in Reference 1 for both nose and shoulder locations are used in this study. Most of the inside surface of the spacecraft structure was covered by a multilayer blanket insulation; therefore the backface boundary condition is taken to be insulated with a heat transfer coefficient of zero. The flight data shows variations in initial temperature from one location to another; however, the temperature gradient across the TPS thickness at a given location was negligible. Therefore, the initial thermocouple measurement from the flight data is used as the initial temperature of the entire TPS block at each location. The surface boundary conditions are defined using option 1 in FIAT for the entire trajectory which includes convection, reradiation and surface chemistry terms in the surface energy balance. Reradiation is modeled to an environment with an effective temperature of 180 K (consistent with the reconstructed atmospheric temperature). The surface boundary conditions (heat transfer coefficient $C_H$, recovery enthalpy $H_r$, and pressure) are derived by spline interpolation of the conditions at the trajectory points where CFD calculations are performed. Spherical geometry with nose radius is used for the nose location while a cylindrical geometry with corner radius is used for the shoulder location. A blowing correction parameter of 0.5 is used for the nose which is consistent with the laminar assumption. The blowing parameter is switched to 0.3 for the shoulder to account for the transition to turbulence.

*3. Comparison to Flight Data*

Figure 9 shows the subsurface FIAT temperature predictions compared to the flight data for the nose and shoulder locations. These results can be compared to the results from the previous analysis done by Milos et. al. shown in Figure 3 and Figure 4. For nose, in the current analysis, the FIAT predictions exceed the flight data for the entire time span; while in the previous analysis, FIAT under predicts the data up to about 100 s and then rises abruptly. This behavior can be partly due to the fact that in the analysis by Milos et. al. the heat transfer coefficient was extrapolated to zero at 20 s and 101 s while in this study they are spline interpolated to a small value at 0 s and 186 s. In the same figure, we can see the subsurface FIAT temperature predictions compared to the flight data for the shoulder location. The same trends observed for the nose can be also seen for the shoulder location. However, at the shoulder, the previous analysis over predicts the data more than the current analysis. It should be noted that there remains some uncertainty with the substructure aluminum honeycomb properties at the shoulder location. In addition, these results may be impacted by the validity of using 1-D conduction at shoulder. Overall the nose FIAT predictions are within 35 K of the flight data while the shoulder predictions are within 25 K of the data. The Root Mean Square (RMS) residuals for the nose and shoulder temperature response with respect to flight data are respectively 19.97 K and 15.33 K. In the previous analysis, the entire heat transfer coefficient profile was scaled to

achieve a better match with the data. In this study we will perform a time-dependent estimation of the heat transfer coefficient which results in a closer match with the flight data (detailed in the Inverse Analysis section).

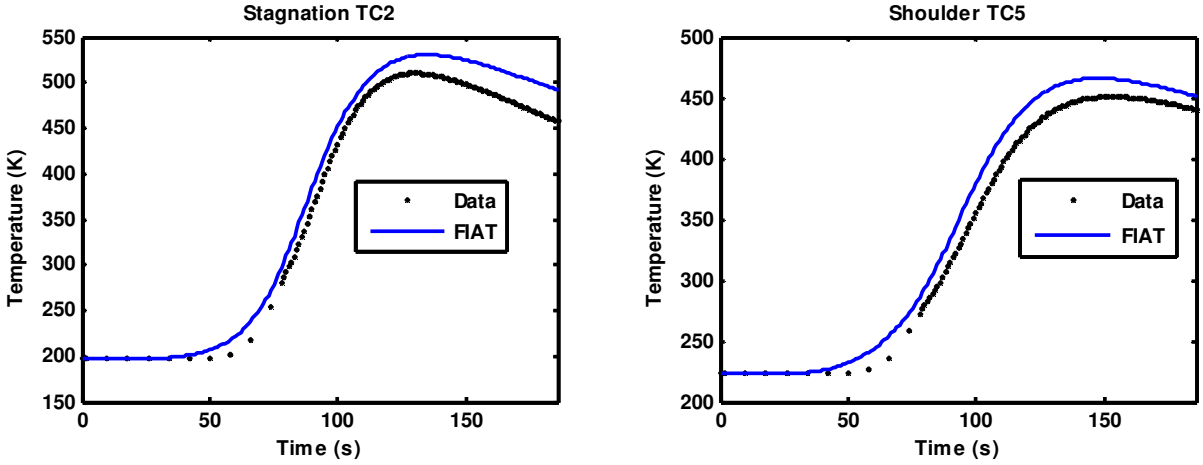


**Figure 9. Pathfinder's nose and shoulder subsurface FIAT temperature predictions compared to flight data**

Figure 10 shows the heat rate profile for both the nose and shoulder locations. Both the FIAT-calculated net surface heat rates and the CFD-calculated heat rates are shown. There are noticeable discrepancies between the radiative equilibrium wall assumption used in CFD and the heating profile extracted from FIAT solutions that used the CFD inputs. These discrepancies are due to two important effects. First, FIAT solves a general surface energy balance that includes in-depth conduction. Thus, after the pulse, the FIAT surface temperatures are higher than CFD predictions and the heating is lower. Second, the CFD simulations assume a constant surface emissivity of 0.85, whereas the updated SLA-561V model lowers the emissivity from 0.85 to 0.5 above 2000 K to address glass melt flow[16]. The FIAT shoulder heat rates are close to CFD as the predicted surface temperatures there do not exceed 2000 K.

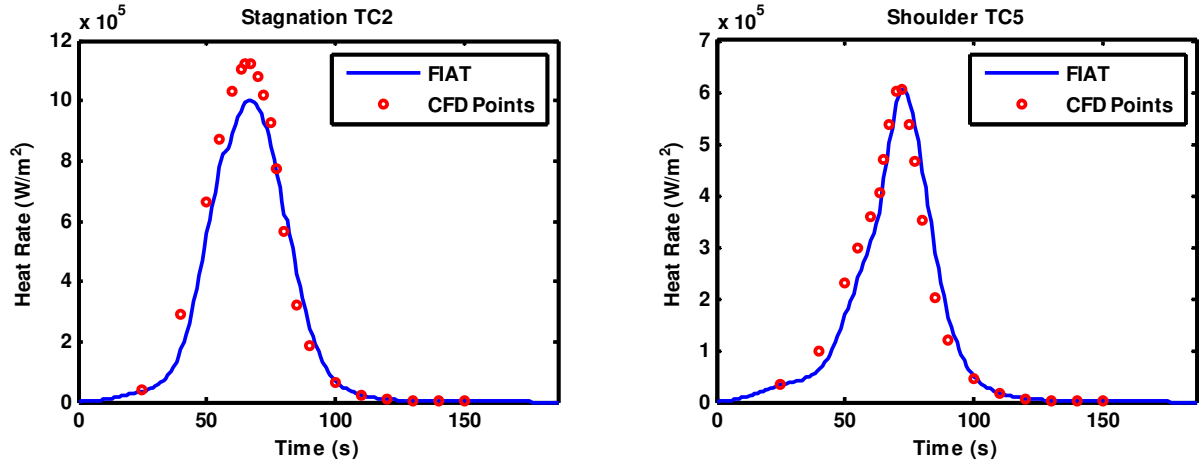


**Figure 10. FIAT-calculated heat rate profiles and CFD-calculated points for the Pathfinder vehicle**

## V. Inverse Analysis

Most engineering problems are posed for direct analysis, where a physical phenomenon is studied using an analytical model. Model parameters and boundary conditions are known and the goal is to compute the system response or model outputs. In section IV, we performed a direct analysis to calculate the in-depth heatshield temperature response using the current best modeling approaches and compared the results with flight data. Analysis of experimental data can be approached in an inverse fashion, if the measurements of a system's response are

available. In this section, we inversely estimate the heatshield boundary conditions from the flight data, achieving a closer match between the FIAT predictions and flight data.

### A. Inverse Problems Background

Inverse problems are mathematically ill-posed meaning that the conditions of solution existence, uniqueness and stability are not generally satisfied. These problems tend to be unstable and sensitive to random or bias errors. Furthermore, different inputs to the model could result in similar model outputs. Therefore, the estimation of boundary conditions from measurements of model outputs is not guaranteed to have a unique solution. Such instabilities could result in large oscillations in the estimated boundary conditions. Regularization techniques are used to redefine the problem such that the new problem is better posed. Inverse methods have been widely used to solve data analysis problems in a broad range of fields such as heat transfer,[17-26] geophysics,[27] trajectory reconstruction,[7-9, 28] remote sensing, mathematics and astronomy. The general methods used in these fields are very similar. In this work we focus on the methods used to solve Inverse Heat Transfer Problem (IHTP).

IHTPs can be categorized in many different ways.[24] They can be classified in accordance with the nature of the dominant heat transfer process: conduction, convection or radiation. Another classification is based on the type of parameters being estimated: boundary conditions,[19] model parameters (material properties),[22] initial conditions or geometric characteristics. This makes the inverse problem either a parameter estimation or function estimation problem. Another classification is based upon the differential equations representing the problem: linear or nonlinear. The spatial and temporal dependence of material properties makes the heat conduction problem nonlinear. The inverse methods used for these problems can also be classified based on the time domain of the measurements used in the estimation process: whole time-domain or sequential. Other ways of classification include the dimension of the heat transfer problem (ex.: 1-D, 2-D or 3-D) and the method of solution of the direct heat transfer problem (ex.: finite difference, finite element, finite control volume, Duhamel's theorem). This investigation is concerned with the category of nonlinear Inverse Heat Conduction Problems (IHCP) for the estimation of boundary conditions. The direct problem is solved using FIAT which is a one-dimensional finite difference code.

The two main methods used for the solution of IHCPs are the whole-time domain method and the sequential function specification method. The whole-time domain methods estimate all of the parameters characterizing the boundary condition profile at the same time using all measurements. The estimation is done by iterative minimization of an objective function S (ordinary least-squares), which is equal to the sum of the square of errors between the measurements and the corresponding temperature predictions. Different methods can be used to perform the minimization such as Gauss-Newton,[22, 25] Levenberg-Marquardt,[24] Box-Kanemasu[22] and different variations of the Conjugate Gradient method.[24] The Gauss-Newton method provides the fastest convergence; however, it can be unstable. In this paper we use this method and resolve the instability problem with the use of regularization techniques. As explained before inverse problems are ill-posed and become unstable in the presence of errors and for small time steps. This can result in large oscillations in the boundary condition estimates. Regularization approaches have to be used in conjunction with the minimization scheme to make the problem better posed and more stable. Regularization has a smoothing effect on the parameter estimates. Russian mathematician Andrey Tikhonov devised a procedure for the regularization of ill-posed problems.[20, 21] His technique involves the addition of a penalty function to the ordinary least-squares function to alleviate oscillations in the solution. By doing this, we are effectively solving a neighboring problem that has solution close to the solution of the original problem, with the distinction that the new problem is better posed. The regularization term can take many different forms.

Unlike whole-time domain methods, sequential methods estimate a given parameter using only a limited range of measurements and continue sequentially in time. One of the leading methods is the function specification method with future time algorithm developed by James Beck.[19] In this method the boundary condition at a given time is estimated using TC measurements for only a limited future time window. Then the solutions are saved and the method continues to the next time step. The number of future time steps used in the estimation has the same effect as the regularization approach used for the whole-time domain methods. This method has the advantage of being more computationally efficient than whole-time domain methods, but less stable. However, to benefit from this efficiency, the code used to solve the direct problem must be able to save and restart the solution in time. FIAT does not currently offer this option. For this reason and the higher stability of whole-time domain methods, they are used for this study. The authors have previously applied inverse methods to the analysis of ground arc jet data and simulated flight data for ablative materials. A comprehensive inverse parameter estimation methodology for the analysis of the aeroheating and TPS experimental data has been developed and was applied to an arc jet dataset.[17] Furthermore, the

authors have investigated the application of inverse methods to the similar problem of MSL's surface heating estimation from simulated MISP data.[18]

## B. Inverse Methodology

In the following section, the estimation problem is defined and the inverse methods used in this study are explained.

### *1. Definition of the Estimation Problem*

Similar to all inverse problems, the Pathfinder data analysis problem has three parts: data, model and estimation parameters. In this case the data consist of the TC2 at nose and TC5 at shoulder which will be analyzed separately. The model used is FIAT. The third component of an inverse problem is the set of model input parameters that will be estimated. The goal of this study is to estimate Pathfinder's time-dependent surface heat flux from the data by matching the model predictions with the flight measurements. However, for an ablative material, heat flux is not a direct input to FIAT. Instead, the following surface energy balance equation is solved:

$$C_H\left(H_r-\left(1+B'\right)h_w\right)+\dot{m}_g h_g+\dot{m}_c h_c+\alpha_w q_{rad}-\sigma\varepsilon_w\left(T_w^4-T_\infty^4\right)-q_{cond}=0 \tag{1}$$

The above equation includes terms representing many of the complex processes that occur at the surface of an ablative material. These terms include the incoming convective heating, the incoming radiation from the shock layer, the reradiation from the TPS material, the material response through pyrolysis and ablation processes and the heat conducted into the TPS material. The recovery enthalpy $H_r$, surface pressure, radiative heating $q_{rad}$, blowing correction, and the unblown heat transfer coefficient $C_H$ are inputs to FIAT environment file as a function of time. The B' tables and gas enthalpy are also inputs to FIAT. The boundary layer convective heating is represented by the first term in the above equation. It is not possible to estimate all the terms in the above equation. Therefore we have to pick the most relevant parameter. In this study, we estimate the unblown heat transfer coefficient $C_H$ which is the main contributor to the incoming convective heating. The other parameters are assumed to be known with low uncertainty. Once the heat transfer coefficient is estimated the resulting heat flux can be calculated using the other parameters. The surface heat flux is the sum of the first three terms in the above equation.

The heat transfer coefficient is a time-dependent parameter. In the previous analysis by Milos et al. the entire CFD-calculated heat transfer coefficient profile was simply manually scaled until a close match between the data and thermal response predictions was reached. However in this study we treat $C_H$ as time-dependent variable and we attempt to estimate it from the flight TC data as a function of time. In this study, $C_H$ is discretized every 2.5 seconds. This is a balance between the desire to have a higher resolution $C_H$ profile, the computational resources and the stability of the inverse methods. The flight data is available from 0 to 186 seconds; therefore we perform the estimation for the same range of $C_H$ profile. The set of estimation parameters is therefore a vector of discretized $C_H$ values corresponding to discrete time points.

### *2. Inverse Methods*

Inverse methods perform estimation by adjusting the surface boundary conditions in order to achieve a close match between FIAT predictions and the data. Since we use a whole-time domain method, all the parameters are estimated simultaneously using all the flight data. The Gauss-Newton algorithm is widely used to solve nonlinear least-squares problems.[22, 24] It is a modification of Newton's method which does not require the knowledge of second derivatives. The algorithm iteratively minimizes the ordinary least-squares objective function S, which is equal to the sum of square of differences between measurements and temperature predictions shown below in matrix form at iteration *k*:

$$S\left(\mathbf{P}^k\right)=\left[\mathbf{Y}-\mathbf{T}\left(\mathbf{P}^k\right)\right]^T\left[\mathbf{Y}-\mathbf{T}\left(\mathbf{P}^k\right)\right] \tag{2}$$

where P is the vector of parameters being estimated (discretized $C_H$ values), Y is the vector of thermocouple flight data and T is the corresponding vector of FIAT temperature predictions. The Gauss-Newton method is developed by deriving the gradient of the above equation, linearizing the vector of predicted temperatures, T(P), with a Taylor series expansion around the current solution, $P^k$, and setting the gradient of S to zero. The expression can be rewritten to derive the change in parameters, $\Delta P$, required to minimize S:

$$\mathbf{J}^{k\,T}\mathbf{J}^{k}\ \Delta\mathbf{P}^{k} = \mathbf{J}^{k\,T}\ \left[\mathbf{Y} - \mathbf{T}\left(\mathbf{P}^{k}\right)\right] \tag{3}$$

where J is the Jacobian matrix which is equal to the derivative of the predicted TC temperatures to estimation parameters (discretized points along the $C_H$ profile) as shown in the equation below:

$$\mathbf{J} = \begin{bmatrix} \dfrac{\partial T_1}{\partial P_1} & \cdots & \dfrac{\partial T_1}{\partial P_N} \\ \vdots & & \vdots \\ \dfrac{\partial T_M}{\partial P_1} & \cdots & \dfrac{\partial T_M}{\partial P_N} \end{bmatrix} \tag{4}$$

where *M* is the number of measurements and *N* is the number of estimation parameters. The calculation of this Jacobian matrix is where most of the inverse problems difficulties arise and is computationally expensive because its numerical approximation requires *N* solutions of the direct problem. This procedure is continued until a stopping criterion is reached. A range of convergence criteria can be used for this problem. Iteration can be stopped when S reaches a small number or when the percent or absolute change in S is small. Another criterion could be to stop the iteration once the absolute or percent change in estimation parameters is smaller than a specified value. A maximum number of iteration is another criterion. These criteria are all implemented in the inverse code; however in the presence of errors they might never be satisfied because the objective function cannot be reduced to small numbers. An approach widely used in literature is the discrepancy principle in which the iteration is stopped once S reaches the expected error in the data.[23] This would be equal to $M\sigma^2$ where $\sigma$ is the standard deviation of the measurement errors. This approach is useful when the errors are known and are normal and have a constant standard deviation. However, in reality this assumption is not always valid. Furthermore, if measurements have bias error this approach cannot be used. Therefore in this work, the iterations are continued for a specified maximum number and the best estimate is taken to be when the solution is stable.

*3. Tikhonov Regularization*

Tikhonov technique is used to regularize the ill-posed inverse problem and alleviate the non-physical oscillations that occur in the boundary condition estimate.[19, 20] First order Tikhonov regularization has proved to be the most effective for the surface heating estimation problems and is therefore used here. The penalty function added is the sum of square of differences between the consecutive $C_H$ values. Equations 2 and 3 need to be modified accordingly:

$$S = \left[\mathbf{Y} - \mathbf{T}\right]^T \left[\mathbf{Y} - \mathbf{T}\right] + \mu \left[\mathbf{H1} \times \mathbf{P}\right]^T \left[\mathbf{H1} \times \mathbf{P}\right] = \sum_{i=1}^{M} \left(Y_i - T_i\right)^2 + \mu \sum_{j=1}^{N-1} \left(P_{j+1} - P_j\right)^2 \tag{5}$$

$$\left[\mathbf{J}^T\mathbf{J} + \mu\,\mathbf{H1}^{\mathbf{T}}\mathbf{H1}\right]\Delta\mathbf{P} = \mathbf{J}^T\ \left[\mathbf{Y} - \mathbf{T}\right] \tag{6}$$

$$\mathbf{H1} = \begin{bmatrix} -1 & 1 & 0 & \cdots & 0 \\ 0 & -1 & 1 & \cdots & 0 \\ \vdots & \ddots & \ddots & \ddots & \vdots \\ 0 & \cdots & 0 & -1 & 1 \\ 0 & 0 & \cdots & 0 & 0 \end{bmatrix} \tag{7}$$

Small values of μ ensure rapid minimization of the ordinary least-squares function, but result in large oscillations in the $C_H$ profile. Larger values of μ reduce oscillations, but slow down the minimization of the objective function. There are different methods and criteria in the literature for the selection of this parameter. The general approach used here is to start with a small value of μ and increase it until the obtained estimate is satisfactory and the degree of oscillations is reduced sufficiently. Qualitatively a good solution is a solution that traces through the unregularized oscillatory solution. The μ values that worked for this problem ranged from $10^9$ to $10^{11}$. This might seem too large compared to the values seen in literature, but it should be noted that most of the work in literature involves the estimation heat flux which is orders of magnitude greater than $C_H$.

### C. Boundary Condition Estimation Results

The plots in Figure 11 show the $C_H$ estimation results for the nose location. The red and blue traces correspond to the nominal CFD-calculated heating conditions and the inversely estimated heating conditions. Plot (a) and (b) show the $C_H$ profile and the corresponding surface heat rate profile for both nominal and reconstructed environments. Plot (c) compares the nominal and estimated in-depth temperature predictions with the flight data at the nose TC location. Finally, plot (d) shows the residual of in-depth temperature response with respect to the flight data for the nominal and reconstructed environments.

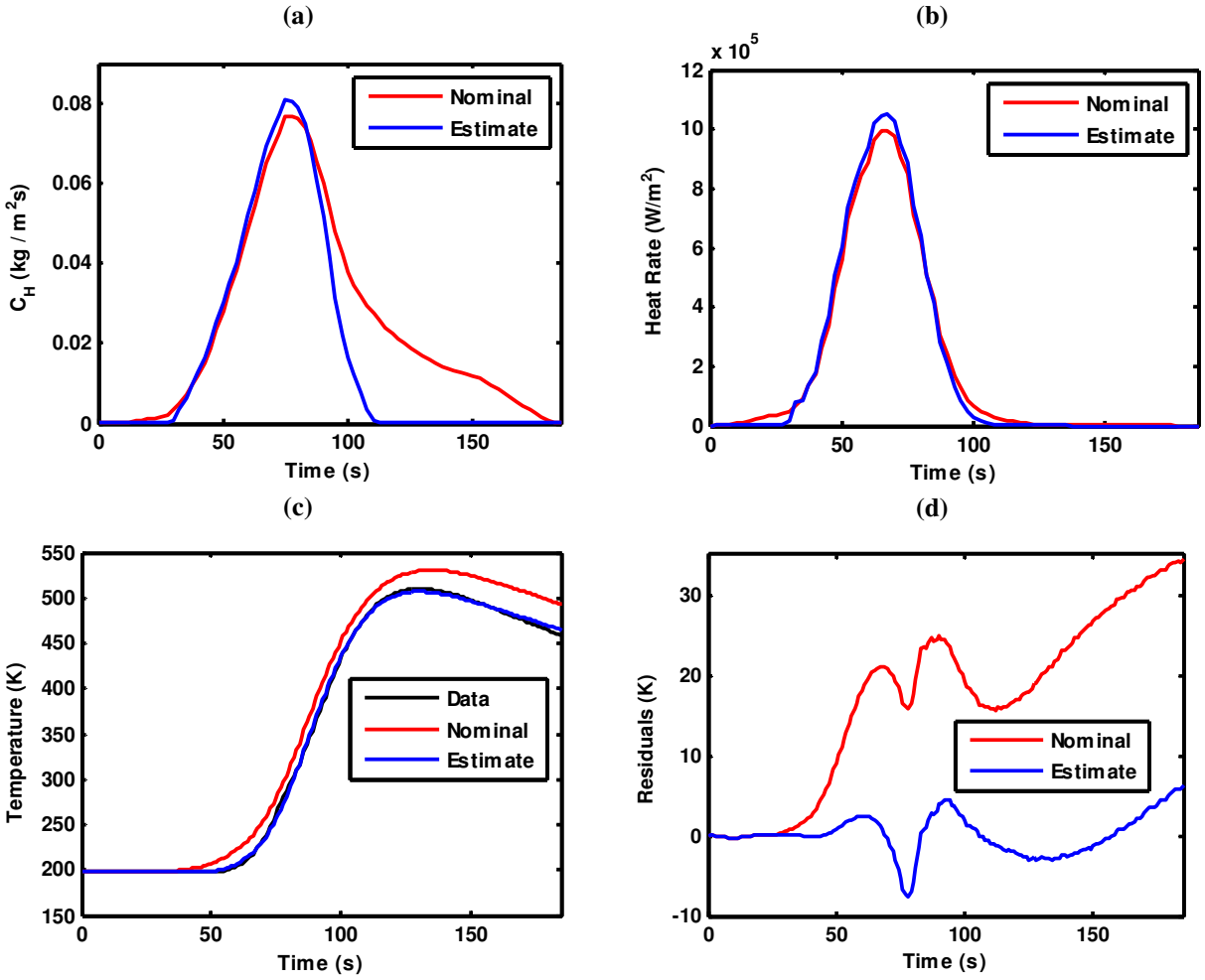


**Figure 11. $C_H$ estimation results for the nose TC location**

In Figure 11 plots (c) and (d) we can clearly observe that after the inverse estimation of $C_H$, FIAT predictions match very well with the data. The maximum difference is reduced to within 7 K of the flight data from the original 35 K. The temperature response RMS residual with respect to flight data is reduced to 2.50 K from the original 19.97 K. The objective function (sum of square of errors between FIAT temperatures and flight data) is reduced by almost two orders of magnitude. In Figure 11 plot (a), we can see that in order to achieve an agreement with the data the estimator attempts to reduce $C_H$ to very small values in the pre-pulse and post-pulse regions of the $C_H$ profile while slightly increasing it in the rising region of the heat pulse.

Figure 12 shows the $C_H$ estimation results for the shoulder location. In plots (c) and (d) we can clearly observe that after the inverse estimation of $C_H$, FIAT predictions match very well with the data. The maximum difference is reduced to within 5 K of the flight data from the original 25 K. The temperature response RMS residual with respect to flight data is reduced to 2.20 K from the original 15.33 K. The objective function is reduced by almost a factor of 40. In plot (a) we can observe that in order to match the data, the estimator reduced the pre-pulse $C_H$ to very small

values and reduced the rising region of the pulse by about 5%. The decreasing regions of the pulse and the post-pulse $C_H$ region have not been changed significantly from CFD predictions. However, there is higher uncertainty at the shoulder due to uncertainty in the substructure material properties, and the limitations of the 1-D conduction effects in this high-gradient region. It should be noted that the results achieved through inverse estimation for both shoulder and stagnation point (±5 K, ±7 K) are better than matches between the new SLA-561V model and arc jet data it is based on, particularly in cool-down (see TC3 and TC4 in Reference 16, Figures 23 and 24). Also according to Reference 1, the TC data are accurate within ± 2 K.

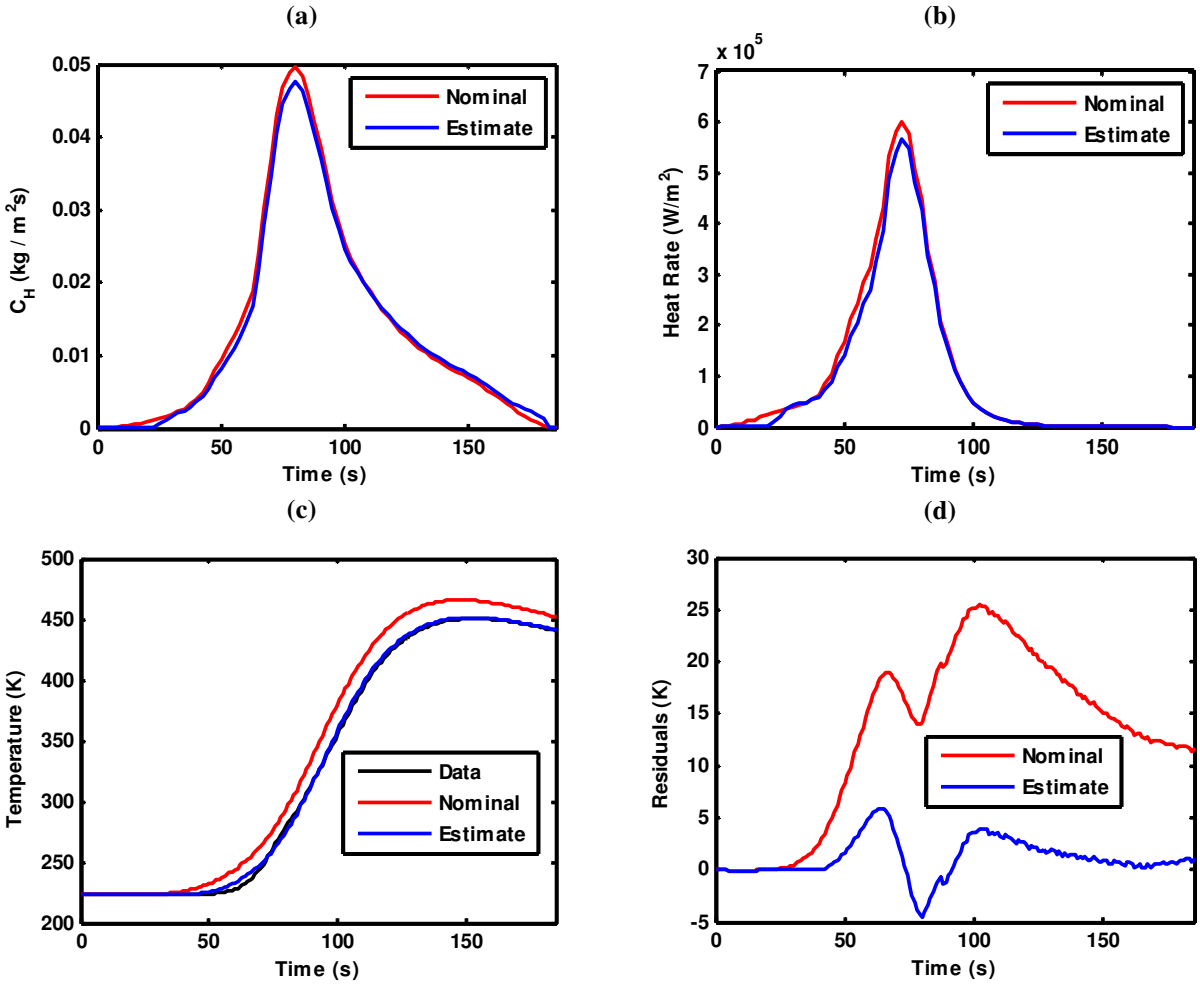


**Figure 12. $C_H$ estimation results for the shoulder TC location**

Inverse estimate and nominal environments from this study are compared to digitized environments from Reference 1 at the nose (TC2) and shoulder (TC5) locations. We observe that the nominal thermal response from new CFD performed over-predicts the temperature, whereas both the inverse estimate and Reference 1 environments result in a good match with the data (Figure 13). Visually, these $C_H$ profiles appear similar, though there are other differences in these environments besides just $C_H$, such as the trajectory and the enthalpy profile. It is thought that some differences in the enthalpy profile are due to limitations in older versions of FIAT that constrained the recovery enthalpy to be positive. However, our conclusion is that the Milos et. al[1] environments, combined with the new SLA-561V material model match the TC2 data well without any scaling of the heat rate. Furthermore, the inversely estimated environments results in a better match with the data, particularly between 50-75 seconds.

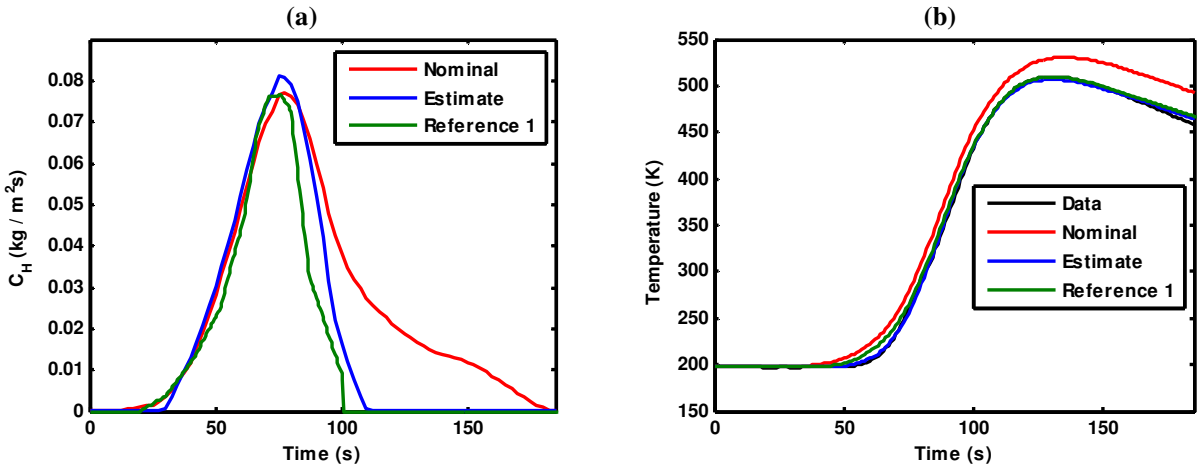


**Figure 13. $C_H$ estimation results for the nose location, including predictions from Milos et. al[1]**

At the shoulder location (Figure 14), we find that the inversely estimated environments result in the best match with the data, with a reduction of pre-pulse $C_H$, and peak reduction of around 5%.

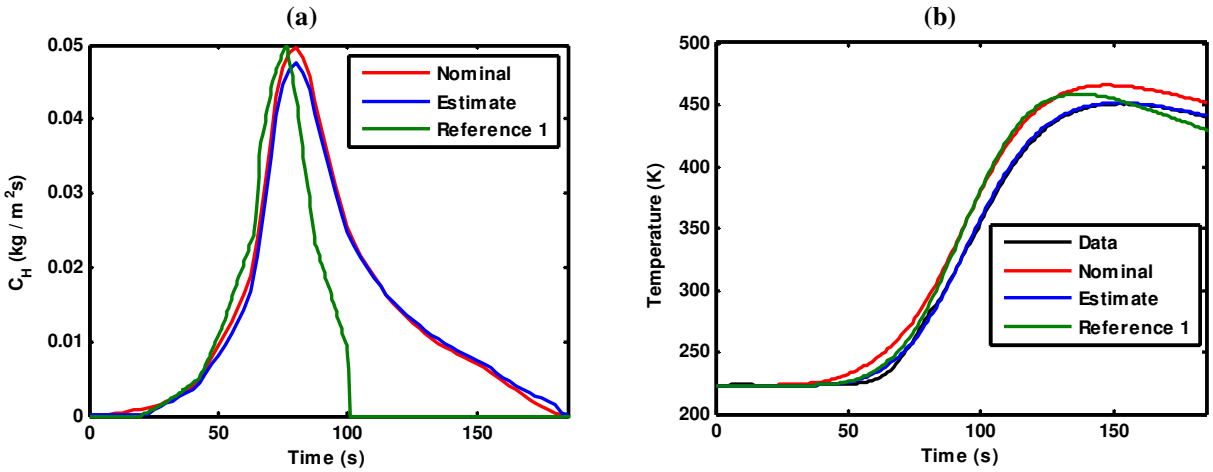


**Figure 14. $C_H$ estimation results for the shoulder location, including predictions from Milos et. al[1]**

## VI. Summary & Conclusions

In this paper, the Mars Pathfinder aerothermal environment and heatshield material response are reconstructed using updated modeling tools and approaches. A newly computed reconstructed trajectory is used. This trajectory is expected to be closer to the true trajectory because the reconstruction weights the more certain altimeter data. Updated CFD simulations were performed using DPLR for selected points along the reconstructed trajectory to characterize the vehicle's heating environment. The shoulder environments employed a turbulence model with transition. The heating boundary conditions were used with the thermal response code FIAT to calculate the forebody heatshield in-depth temperature response at the location of nose and shoulder mid-depth thermocouples. An updated thermal response and ablation model for the TPS material, SLA-561V, was used in this study. The direct FIAT predictions match the general trend of the flight data with a maximum difference of 35 K for the nose and 25 K for the shoulder locations.

In addition to this direct comparison, the analysis was also done in an inverse fashion. Inverse methods, specifically the Gauss-Newton minimization algorithm in conjunction with Tikhonov regularization technique, were employed to reconstruct the time-dependent unblown heat transfer coefficient by minimizing the difference between the FIAT predictions and flight data. The estimator was able to reconstruct the $C_H$ profile such that the

corresponding temperature response was a good match with the flight data. The maximum difference was reduced to 7 K for the nose and 5 K for the shoulder. In order to achieve this close match for the nose location, the estimator reduced the pre-pulse and post-pulse $C_H$ profile to very small values while slightly increasing it in the rising region of the pulse. This demonstrates an advantage of inverse methods where the surface properties can be estimated as a function of time and are not limited by a simple uniform scaling. In order to match the TC data at the shoulder location, the estimator reduced the pre-pulse $C_H$ to small values while maintaining the post-pulse $C_H$ and slightly decreasing the peak value. This inverse solution at the shoulder is plausible. However, there is higher uncertainty here due to uncertainty in the substructure materials and the limitations of the 1-D conduction effects in this high-gradient region. [1, 14]

The study of bondline TC data was excluded from this paper because it differed greatly from thermal response model predictions. Similar observations have been made for thermocouples close to bondline in ground testing. In order to use such TC data from future flight instrumentation (ex. MISP), we need to understand and be able to model the cause of the pre-heating trend observed in the bondline TCs. In this study, the importance of an accurate knowledge of substructure material properties has been demonstrated. Therefore, it is important that these properties are determined accurately for future analysis of flight instrumentation data.

In general, it seems that the CFD models perform a good job of predicting the heating conditions in the heat pulse region, but not accurately in the off-pulse regions. Furthermore, it seems that the starting and ending values used in spline interpolation for CFD should be revisited, as they can result in an overestimation of the heating conditions in the off-pulse regions. It should be noted that in the previous analysis by Milos et al. this interpolation was not done and the heat transfer coefficient was set to zero in the beginning and end regions of the trajectory. Considering this, we can conclude that the updated SLA ablation and thermal response, combined with the inverse solution techniques, are the main contributors to the improved agreement with the data observed in this analysis.

Iterative coupling between CFD and current material response codes may improve the match between CFD predictions and inverse reconstructed environments. This would largely eliminate the heat rate discrepancies due to conduction and emissivity difference noted previously. Also, blowing of ablation products could also be included in the DPLR simulations (such as Reference 14), though this would substantially increase the complexity and computational cost of the inverse analysis process. Inverse analysis revealed a strong dependence of the reconstructed shoulder environment to substructure properties. For the current analysis, there are uncertainties in the thermal properties of the filled aluminum honeycomb. In addition to the material uncertainties, we expect 1-D conduction modeling may not be sufficient for the shoulder region where there is both high curvature and strong heat rate gradients along the surface. An inverse analysis process coupled with a 2-D material response code could increase confidence in the shoulder results, though with an associated increase in computational cost.

## Acknowledgments

This work was funded by the NASA grant NNX12AF94A from the NRA Research Opportunities in Aeronautics 2010. Portions of this work were conducted under NASA contract NNA10DE12C to ERC, Incorporated. The authors would like to thank Soumyo Dutta for providing the reconstructed Pathfinder trajectory. The authors are grateful to Bernard Laub, Deepak Bose, Frank Milos, Y.-K. Chen, Ioana Cozmuta, Michael Wright, and David Hash for their time to discuss some aspects of this work.

## References

[1] Milos, F., Chen, Y.-K., Congdon, W., and Thornton, J., "Mars Pathfinder Entry Temperature Data, Aerothermal Heating, and Heatshield Material Response," *Journal of Spacecraft and Rockets*, Vol. 36, No. 3, 1999, pp. 380– 391.

[2] Wright, M., Chun, T., Edquist, K., Hollis, B., Krasa, P., and Campbell, C., "A Review of Aerothermal Modeling for Mars Entry Missions," *48th AIAA Aerospace Sciences Meeting*, AIAA 2010-443, January 2010.

[3] Gazarik, M., Wright, M., Little, A., Cheatwood, F. M., Herath, J., Munk, M., Novak, F., and Martinez, E., "Overview of the MEDLI Project," IEEE 2008-1510, *IEEE Aerospace Conference*, Big Sky, Montana, March 2008.

[4] Wright, M. J., Candler, G. V., and Bose, D., "Data-Parallel Line Relaxation Method of the Navier-Stokes Equations," *AIAA Journal*, Vol. 36, No. 9, 1998, pp., 1603-1609.

[5] Chen, Y.K., and Milos, F.S., "Ablation and Thermal Response Program for Spacecraft Heatshield Analysis", *Journal of Spacecraft and Rockets*, Vol. 36, No. 3, 1999, pp. 475-483.

[6] Laub, B., "The Mysteries of Real Materials," *5th Ablation Workshop*, Lexington, Kentucky, February 28 – March 1, 2012.

[7] Spencer, D. A., Blanchard, R. C., Braun, R. D., Kallemeyn, P. H., and Thurman, S.W., "Mars Pathfinder Entry, Descent, and Landing Reconstruction," *Journal of Spacecraft and Rockets*, Vol. 36, No. 3, 1999, pp. 357–366.

[8] Dutta, S., and Braun, R.D., "Mars Entry, Descent, and Landing Trajectory and Atmosphere Reconstruction," *48th AIAA Aerospace Sciences Meeting*, AIAA 2010-1210, January 2010.

[9] Christian, J., Verges, A., and Braun, R., "Statistical Reconstruction of Mars Entry, Descent, and Landing Trajectories and Atmospheric Profiles," *AIAA SPACE Conference and Exposition*, AIAA 2007-6192, Long Beach, CA, 2007.

[10] White, T., Cozmuta, I., Santos, J., Laub, B., Mahzari, M., "Proposed Analysis Process for Mars Science Laboratory Heat Shield Sensor Plug Flight Data," *42nd AIAA Thermophysics Conference*, AIAA 2011-3957, Honolulu, Hawaii, June 27-30, 2011.

[11] Szalai, C., Thoma, B., Lee, W., Maki, J., Willcockson, W., Venkatapathy, E., and White, T "Mars Exploration Rover Heatshield Observation Campaign," *42nd AIAA Thermophysics Conference*, AIAA 2011-3956, Honolulu, Hawaii, June 27-30, 2011.

[12] "ASI/MET Derived EDL Density/Pressure/Temperature Profiles," MPFL-M-ASIMET-4-DDR-EDL-V1.0, mpam_0001/edl_ddr, NASA Planetary Data System, April 1999.

[13] Mitcheltree, R.A. and P.A. Gnoffo, "Wake Flow About a MESUR Mars Entry Vehicle," AIAA 94-1958, June 1994.

[14] Chen, Y.-K., Henline, W.D., and Tauber, M.E., "Mars Pathfinder Trajectory Based Heating and Ablation Calculations", *Journal of Spacecraft and Rockets,* Vol. 32, No. 2, 1995, pp. 225-230.

[15] Brown, J.L., "Turbulence Model Validation for Hypersonic Flows," AIAA 2002-3308, June 2002.

[16] Laub, B., Chen, Y.K., Dec, J.A., "Development of a High-Fidelity Thermal/Ablation Response Model for SLA-561V," *41st AIAA Thermophysics Conference*, AIAA 2009-4232, San Antonio, Texas, June 2009.

[17] Mahzari, M., Cozmuta, I., Clark, I., Braun, R., "An Inverse Parameter Estimation Methodology for the Analysis of Aeroheating and Thermal Protection System Experimental Data," *42nd AIAA Thermophysics Conference*, AIAA 2011-4027, Honolulu, Hawaii, June 27-30, 2011.

[18] Mahzari, M., Braun, R. D., "Time-dependent Estimation of Mars Science Laboratory Heat Flux from Simulated MEDLI Data ," to be submitted for the *43rd AIAA Thermophysics Conference*, New Orleans, Louisiana, June, 2011.

[19] Beck, J.V., Blackwell, B., and St. Clair, C.R., *Inverse Heat Conduction, Ill-posed Problems*, Wiley, New York, 1985.

[20] Tikhonov, A. N., and Arsenin, V. Y., *Solution of Ill-Posed Problems*, Winston & Sons, Washington, DC, 1977.

[21] Tikhonov, A. N., Leonov, A. S, and Yagola, A. G., *Nonlinear Ill-posed Problems*, Chapman & Hall, London, 1998.

[22] Beck, J.V., and Arnold, K. J., *Parameter Estimation in Engineering and Science, Wiley, New York, 1977.*

[23] Alifanov, O. M., *Inverse Heat Transfer Problems*, Springer-Verlag, New York, 1994.

[24] Özisik, M. N., and Orlande*,* H. R. B.*, Inverse Heat Transfer: Fundamentals and Applications,* Taylor and Francis, New York, 2000.

[25] Woodbury, K. A., *Inverse Engineering Handbook*, CRC Press, Boca Raton, 2003.

[26] Kurpisz, K. and Nowak, A. J., *Inverse Thermal Problems*, WIT Press, Southampton, UK, 1995.

[27] Aster, R., Borchers, B., and Thurber, C*., Parameter Estimation and Inverse Problems,* Elsevier Academic Press, Burlington, 2005.

[28] Dutta, S., Braun, R.D., Russell, R.P., Clark, I.G., and Striepe, S.A., "Comparison of Statistical Estimation Techniques for Mars Entry, Descent, and Landing Reconstruction from MEDLI-like Data Sources," *50th AIAA Aerospace Sciences Meeting,* AIAA 2012-0400, Nashville, TN, January 2012.